



37 **1 Introduction**

38 Air quality has become a central indicator of the evolving interaction between climate
39 processes and human activity during the Anthropocene. In rapidly urbanizing regions,
40 particularly within densely populated coastal environments, atmospheric conditions strongly
41 regulate the capacity of the lower atmosphere to disperse pollutants. Persistent exposure to
42 fine particulate matter and toxic gases in large urban agglomerations has been associated
43 with increased rates of cardiopulmonary disease, highlighting the growing societal relevance
44 of atmospheric ventilation processes (Agarwal, 2024).

45 Among the meteorological conditions that control atmospheric dispersion, air stagnation
46 (AS) represents one of the most influential. Stagnation occurs when weak horizontal winds
47 and limited vertical mixing reduce ventilation within the boundary layer, allowing pollutants
48 and heat to accumulate near the surface. Under such conditions, the efficiency of atmospheric
49 renewal declines and urban environments can temporarily function as atmospheric sinks.
50 Observational and modeling studies have shown that stagnation events may substantially
51 amplify pollutant concentrations in densely built environments, particularly within poorly
52 ventilated urban canyons (Sarria et al., 2025; Li et al., 2019; Molina, 2020). When these
53 conditions coincide with thermal inversions, pollutant accumulation intensifies within the
54 lower boundary layer, leading to pronounced increases in particulate matter concentrations
55 (Ryu & Min, 2024). These interactions illustrate that stagnation is not simply a local
56 meteorological anomaly but a key physical mechanism linking atmospheric stability to urban
57 air-quality deterioration.

58 Air stagnation typically develops when persistent high-pressure systems suppress synoptic-
59 scale circulation, weaken both surface and mid-tropospheric winds, and limit precipitation.
60 This combination of factors enhances dynamic stability and reduces vertical and horizontal
61 mixing within the lower troposphere (Leung & Gustafson, 2005; Horton et al., 2014; Tai et
62 al., 2012). To quantify these conditions, Wang and Angell (1999) introduced the Air
63 Stagnation Index (ASI), a composite metric defined by three simultaneous thresholds: near-
64 surface wind speed below 3.2 m s^{-1} , 500-hPa wind speed below 13 m s^{-1} , and daily
65 precipitation below 1 mm. Since its introduction, the ASI has become a widely adopted
66 diagnostic framework for identifying meteorological environments conducive to pollutant
67 accumulation.



68 Numerous studies have demonstrated the close connection between stagnation episodes and
69 air-quality degradation. Early work by Jacob et al. (1999) showed that periods of elevated
70 tropospheric ozone in the United States coincided with pronounced stagnation events.
71 Subsequent analyses indicated that such episodes could increase PM_{2.5} concentrations by
72 several micrograms per cubic meter, representing a substantial environmental and public-
73 health burden (Fiore et al., 2015). Similar relationships have been reported across Europe,
74 where stagnation conditions significantly enhance near-surface concentrations of gaseous
75 pollutants (Ordóñez et al., 2005). Because the ASI isolates meteorological controls on
76 pollutant dispersion independent of emission variability, it provides an objective framework
77 for diagnosing the atmospheric capacity to ventilate polluted air masses (Leung & Gustafson,
78 2005; Horton et al., 2012; Wang et al., 2022; Zhou et al., 2024; Huang et al., 2017). As
79 emphasized by Jacob and Winner (2009), this physical focus makes stagnation metrics
80 particularly valuable for interpreting the climatic drivers of air-quality variability.

81 At larger spatial scales, stagnation frequency has been investigated using global reanalysis
82 datasets. The U.S. National Climatic Data Center (NCDC) adopted the ASI as a standard
83 framework for monitoring atmospheric conditions associated with air-quality deterioration
84 and has produced global maps of stagnation-day occurrence (Horton et al., 2012; Leung &
85 Gustafson, 2005; Zhou et al., 2024). These analyses reveal pronounced regional contrasts.
86 For example, parts of the eastern United States experience more than 100 stagnation days per
87 year, while in China persistent stagnation regimes dominate major continental basins such as
88 the Tarim and Sichuan regions (Huang et al., 2017). Such spatial variability reflects the
89 strong influence of synoptic circulation, regional topography, and large-scale climatic forcing
90 on atmospheric ventilation.

91 Recent research also suggests that climate change may alter the frequency and persistence of
92 stagnation events. Rising surface temperatures and modifications in large-scale circulation
93 patterns have the potential to weaken land–sea pressure gradients and reduce atmospheric
94 ventilation efficiency. Horton et al. (2014) indicated that stagnation frequency could increase
95 in climatically sensitive regions including the Mediterranean basin and East Asia. Additional
96 studies have linked this tendency to broader circulation changes, including a slowdown of
97 upper-level winds and modifications of the Hadley circulation (Seidel et al., 2008; Lu et al.,
98 2007). Within this framework, air stagnation emerges not only as a local meteorological



99 condition but also as a manifestation of evolving large-scale circulation regimes under global
100 climate change.

101 Despite substantial progress in global assessments, the spatial and temporal behavior of
102 stagnation remains poorly documented across the Middle East and North Africa (MENA).
103 This knowledge gap is particularly evident for highly urbanized environments such as the
104 Nile Delta in northern Egypt. The Delta represents a densely populated coastal–continental
105 transition zone characterized by intense urbanization, concentrated industrial activity, and
106 extremely high population density. At the same time, its low-relief geomorphology and open
107 alluvial landscape limit mechanical ventilation within the boundary layer. These
108 characteristics create conditions that may favor persistent stagnation, yet the climatological
109 structure and long-term evolution of this phenomenon in the region remain insufficiently
110 explored.

111 The Nile Delta occupies a climatically sensitive position within the eastern Mediterranean
112 atmospheric system. Regional circulation alternates between Mediterranean cyclonic activity
113 during winter and the dominance of subtropical high-pressure systems during summer. This
114 seasonal transition modulates the balance between horizontal ventilation and vertical mixing
115 within the lower atmosphere (Horton et al., 2012; Huang et al., 2017). Rapid urban
116 expansion and the intensification of the Urban Heat Island (UHI) effect further modify local
117 boundary-layer processes by enhancing surface warming and strengthening near-surface
118 stability (Wang et al., 2021; Raj et al., 2020). Satellite observations have also revealed
119 elevated Aerosol Optical Depth (AOD) and increased dust loading over several Delta cities
120 during stagnant conditions, illustrating the feedback between atmospheric stability and
121 pollutant accumulation (El-Metwally et al., 2010; El-Askary et al., 2006). Together, these
122 factors suggest that the Nile Delta provides a natural setting in which regional circulation,
123 boundary-layer dynamics, and anthropogenic forcing interact to shape stagnation behavior.

124 Despite the environmental and demographic significance of the Nile Delta, no previous study
125 has systematically examined the long-term climatology, spatial structure, and temporal
126 evolution of air stagnation across this region.

127 Building on this scientific gap, the present study provides the first comprehensive
128 climatological assessment of air stagnation dynamics over the Egyptian Nile Delta during the
129 period 1980–2020. The analysis employs the Air Stagnation Index derived from ERA5 and



130 ERA5-Land reanalysis data produced by the European Centre for Medium-Range Weather
131 Forecasts (ECMWF) (Hersbach et al., 2020). Through integrated spatial and statistical
132 analyses, the study pursues three principal objectives: (i) to construct a high-resolution
133 climatology of stagnation frequency and variability across the Nile Delta; (ii) to examine the
134 relationship between stagnation trends and regional circulation variability over the eastern
135 Mediterranean; and (iii) to generate spatio-temporal diagnostics that improve understanding
136 of atmospheric ventilation efficiency and support future applications in air-quality
137 management and sustainable urban planning within deltaic environments.

138 2. Study Area

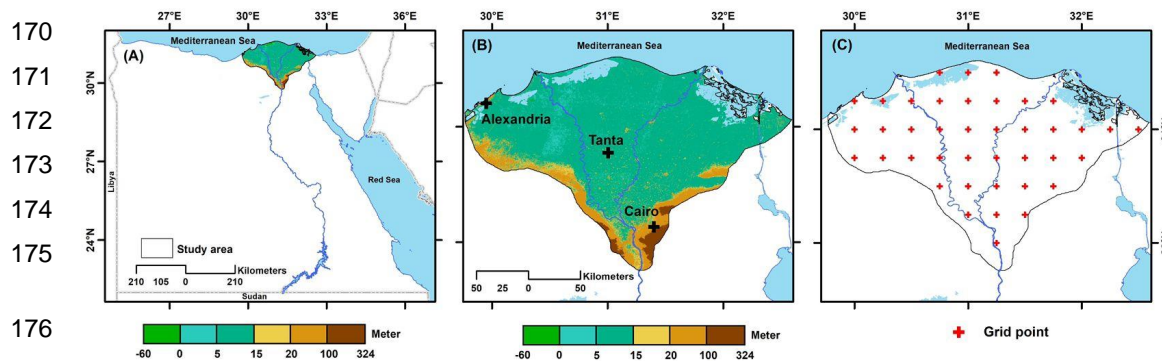
139 The Nile Delta occupies the northernmost part of Egypt and forms the terminal segment of
140 the Nile River's extensive alluvial plain before its discharge into the Mediterranean Sea.
141 Geographically, the Delta extends between latitudes 29°45'–31°36' N and longitudes 29°–
142 32°35' E (Figure 1A). The region spans approximately 220 km from west to east and about
143 170 km from south to north, covering nearly 23,000 km², which represents around 2.3% of
144 Egypt's total land area. Despite this relatively limited spatial extent, the Delta hosts more
145 than 40% of the national population (CAPMAS, 2023; Frihy & El-Sayed, 2013; Stanley &
146 Warne, 1998). This exceptional demographic concentration makes the Nile Delta one of the
147 most densely populated coastal plains within the Mediterranean basin and highlights the
148 environmental relevance of atmospheric conditions affecting the region.

149 The geomorphology of the Delta is characterized by an extremely low-relief surface that
150 developed through long-term fluvial sediment deposition. As illustrated in the elevation
151 model in Figure 1B, most of the Delta plain lies below 20 m above mean sea level and
152 exhibits only a very gentle northward to northwestern slope toward the Mediterranean
153 coastline. The absence of major topographic barriers results in a highly uniform terrain
154 across the region, while minor elevation variations occur mainly along the southern and
155 peripheral margins of the Delta. Several major urban centers, including Cairo, Tanta,
156 Mansoura, and Alexandria, are distributed across this flat alluvial surface (El-Metwally et al.,
157 2010; El-Askary et al., 2006).

158 Climatically, the Nile Delta lies within a Mediterranean–semi-arid transition zone influenced
159 by both maritime conditions from the Mediterranean Sea and continental atmospheric
160 processes over northeastern Africa. Winters are generally mild and relatively humid, whereas



161 summers are hot and predominantly dry. Mean air temperatures typically range between 15–
 162 20 °C during winter and frequently exceed 35 °C in summer. Precipitation exhibits a
 163 pronounced north–south gradient across the Delta, with annual totals generally below 200
 164 mm along the Mediterranean coast and decreasing to less than 50 mm toward inland sectors
 165 (Abdelaal, 2024). Long-term observations further indicate a persistent regional warming
 166 trend of approximately 0.3 °C per decade since the 1970s, accompanied by declining relative
 167 humidity and an increasing coastal–inland humidity gradient. These climatic tendencies are
 168 consistent with broader patterns of progressive aridification reported across the eastern
 169 Mediterranean region (Hassaan & Abdrabo, 2023; IPCC, 2021).



178 Figure 1 Location of the study area and related variables. (A) Nile Delta within northern Egypt,
 179 (B) elevation gradient of the Nile Delta, together with the distribution of weather stations
 180 employed for validation, (C) $0.25^\circ \times 0.25^\circ$ grid points applied for AS analysis

181 At the synoptic scale, the regional atmospheric circulation affecting the Nile Delta is
 182 governed primarily by two alternating systems that dominate different seasons of the year.
 183 During winter, Mediterranean cyclones frequently influence northern Egypt and produce
 184 episodic rainfall events and transient atmospheric disturbances. In contrast, summer
 185 conditions are typically controlled by the subtropical high-pressure belt extending across
 186 North Africa and the eastern Mediterranean, which favors relatively stable atmospheric
 187 conditions over the region (Zanaty et al., 2024). The seasonal alternation between these
 188 circulation regimes contributes to marked variability in atmospheric stability and ventilation
 189 characteristics throughout the year.

190 For the purposes of spatial analysis, the study domain is represented using evenly distributed
 191 grid cells with a spatial resolution of $0.25^\circ \times 0.25^\circ$, as shown in Figure 1C. These grid points



192 provide consistent coverage of the Delta region and form the spatial framework used to
193 examine the distribution and variability of atmospheric stagnation conditions across the study
194 area.

195 **3. Data and Methodology**

196 **3.1 Data**

197 This study is based on atmospheric fields derived from the ERA5 reanalysis produced by the
198 European Centre for Medium-Range Weather Forecasts (ECMWF) and accessed through the
199 Copernicus Climate Data Store. ERA5 provides globally gridded atmospheric variables at a
200 horizontal resolution of $0.25^\circ \times 0.25^\circ$ with hourly temporal resolution extending from 1979
201 onward (Hersbach et al., 2020). The analysis period spans January 1980 to December 2020,
202 ensuring a sufficiently long record for assessing multi-decadal variability in stagnation
203 frequency. The Nile Delta domain was represented using the native ERA5 grid, yielding 40
204 grid cells fully covering the study area (Fig. 1C). These grid cells constituted the
205 fundamental spatial units for all subsequent calculations and statistical analyses.

206 Hourly fields retrieved for each grid cell include:

- 207 • 10-m zonal and meridional wind components (u10, v10)
- 208 • 500-hPa zonal and meridional wind components (u500, v500)
- 209 • Total precipitation

210 Daily precipitation totals were obtained by aggregating hourly precipitation within each
211 calendar day. All spatial processing was conducted in the WGS-84 geographic coordinate
212 system. Consistency across variables and temporal alignment of grid cells were verified prior
213 to computation.

214

215 **3.2 Wind Computation and Temporal Aggregation**

216 Wind speed at both the near-surface (10 m) and mid-tropospheric (500 hPa) levels was
217 calculated from the horizontal wind components according to:

218

$$S = \sqrt{U^2 + V^2}$$

219 Hourly wind components at both the 10-m level (u10, v10) and the 500-hPa level (u500,
220 v500) were retrieved from ERA5. Wind speed was calculated at hourly resolution for each
221 grid cell from the horizontal wind components, and daily mean wind speeds were



222 subsequently derived as the arithmetic mean of the 24 hourly values. The same procedure
223 was applied to both near-surface and mid-tropospheric winds, ensuring that stagnation
224 thresholds were evaluated from dynamically resolved fields rather than from pre-aggregated
225 daily products.

226 **3.3 Air Stagnation Index (ASI)**

227 Air stagnation was diagnosed following the framework of Wang and Angell (1999) and
228 Horton et al. (2012). A stagnation day was identified when, within a given grid cell and
229 calendar day, the following conditions were simultaneously satisfied:

- 230 1. Daily mean 10-m wind speed $< 3.2 \text{ m s}^{-1}$
- 231 2. Daily mean 500-hPa wind speed $< 13.0 \text{ m s}^{-1}$
- 232 3. Daily total precipitation $< 1 \text{ mm}$

233 A day was classified as a stagnation day only when all three ASI thresholds were
234 simultaneously satisfied within the same grid cell and calendar day, ensuring that the
235 diagnosed events represent coherent atmospheric conditions characterized by weak
236 horizontal ventilation, reduced mid-tropospheric flow, and absence of precipitation.

237 Each grid cell was assigned to a binary daily indicator (1 = stagnation; 0 = non-stagnation).
238 Stagnation episodes were defined as sequences of consecutive stagnation days within each
239 grid cell, allowing the identification of event persistence and the quantification of episode
240 duration within the stagnation climatology. From this binary time series, annual and seasonal
241 stagnation frequencies were calculated. Event-based metrics, including mean duration and
242 maximum consecutive stagnation sequence, were derived from continuous runs of stagnation
243 days.

244 **3.4 Validation**

245 ERA5-derived daily surface wind speed at 10 m and daily precipitation were evaluated
246 against independent station observations obtained from the NOAA Global Surface Summary
247 of the Day (GSOD) archive. Three stations representing the coastal–inland climatic gradient
248 of the Nile Delta were selected for the validation analysis: Alexandria, Tanta, and Cairo
249 International Airport. ERA5 grid-point values corresponding to each station location were
250 extracted and temporally matched with the daily GSOD records for the common analysis



251 period (1980–2020). Statistical agreement between the two datasets was quantified using the
252 Pearson correlation coefficient (r), coefficient of determination (R^2), root mean square error
253 (RMSE), mean bias error (MBE), and Willmott’s modified index of agreement (d_1).
254 Statistical significance was assessed at $p < 0.01$.

255 **3.5 Trend Analysis**

256 Temporal trends in stagnation frequency were evaluated using the non-parametric Mann–
257 Kendall test, a widely applied method for detecting monotonic trends in hydro-climatic time
258 series. Prior to trend detection, each time series was examined for serial autocorrelation using
259 the lag-1 autocorrelation coefficient, since positive autocorrelation may inflate the variance
260 of the Mann–Kendall statistic and consequently overestimate trend significance. When
261 significant autocorrelation was detected at the 95% confidence level, the Modified Mann–
262 Kendall procedure proposed by Hamed and Rao (1998) was applied to adjust the variance of
263 the test statistic and ensure a robust assessment of statistical significance. The magnitude of
264 detected trends was quantified using Sen’s slope estimator, which provides a median-based
265 rate of change that is resistant to outliers and non-normal data distributions.

266 Trend magnitudes are expressed in days per decade and were evaluated at both annual and
267 seasonal scales. Statistical significance was assessed at $\alpha = 0.05$. All statistical analyses were
268 performed using Python (version 3.11).

269 **4. Results**

270 Prior to examining the dynamics of air stagnation across the Nile Delta, the reliability of the
271 ERA5 reanalysis was evaluated against independent station observations. Daily
272 meteorological records were obtained from the Global Surface Summary of the Day (GSOD)
273 archive maintained by the National Oceanic and Atmospheric Administration (NOAA). The
274 GSOD dataset compiles quality-controlled surface observations from stations operating
275 within the World Meteorological Organization (WMO) network and provides continuous
276 daily measurements of key meteorological variables, including wind speed and precipitation.

277 A station-based comparison was conducted between ERA5 grid-point values and GSOD
278 observations for three representative stations across the Nile Delta: Alexandria, Tanta, and
279 Cairo Airport, covering the period 1980–2020. ERA5 fields were temporally matched with



280 the corresponding daily GSOD records prior to statistical evaluation in order to ensure
 281 consistency between the two datasets.

282 The comparison demonstrates strong agreement between ERA5 and the GSOD observations.
 283 As summarized in Table 1, correlation coefficients exceed 0.89, coefficients of determination
 284 range from 0.83 to 0.92, and root mean square errors remain below 2 m s^{-1} for wind speed
 285 and 1 mm day^{-1} for precipitation, values that are well within the range commonly reported
 286 for reanalysis validation studies. Scatterplots presented in Figure 2 further illustrate this
 287 agreement, with most data points clustering close to the 1:1 reference line and the fitted
 288 linear regression closely following the same relationship. These graphical patterns are
 289 consistent with the statistical metrics summarized in Table 1 and indicate strong overall
 290 agreement between the two datasets, with only limited systematic bias as reflected by the low
 291 MBE values. Collectively, these validation results demonstrate that ERA5 reliably
 292 reproduces the temporal variability of near-surface wind speed and precipitation across the
 293 Nile Delta, providing a robust foundation for the subsequent climatological analysis of air
 294 stagnation.

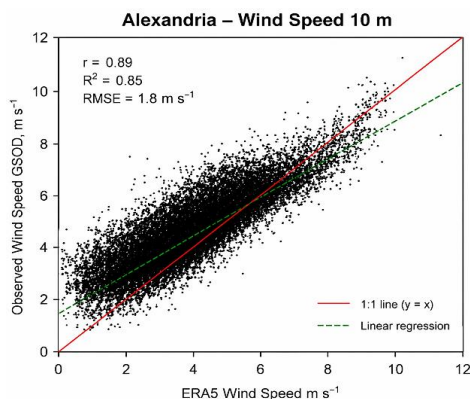
295 Table 1. Statistical validation of ERA5 wind speed and precipitation against GSOD station
 296 observations across the Nile Delta (1980–2020).

Station	Variable	Level	r	R ²	RMSE	MBE	d _i	p-value
Alexandria	Wind speed (m/s)	Surface (10 m)	0.89	0.85	1.8	-0.2	0.91	<0.001
	Precipitation (mm/day)	Surface	0.91	0.86	0.7	0.02	0.90	<0.01
Tanta	Wind speed (m/s)	Surface (10 m)	0.94	0.90	1.9	-0.3	0.90	<0.001
	Precipitation (mm/day)	Surface	0.87	0.83	0.6	0.04	0.92	<0.01
Airport Cairo	Wind speed (m/s)	Surface (10 m)	0.96	0.92	1.6	-0.1	0.93	<0.001
	Precipitation (mm/day)	Surface	0.93	0.90	0.5	0.03	0.92	<0.01

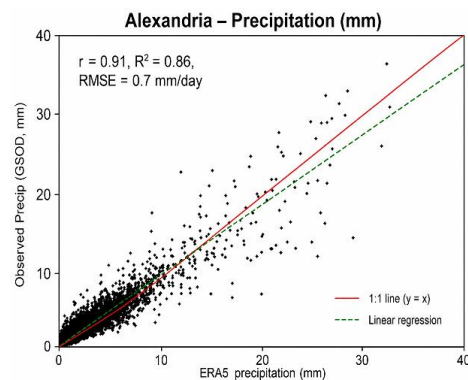
297 Notes: r: Pearson correlation coefficient; R²: coefficient of determination; RMSE: root mean square error;
 298 MBE: mean bias error; d_i: Willmott’s modified index of agreement. All correlations are significant at $p <$
 299 0.01. Validation was performed using temporally matched daily observations from the NOAA Global
 300 Surface Summary of the Day (GSOD) archive for 1980–2020.



301



302



303

304

305

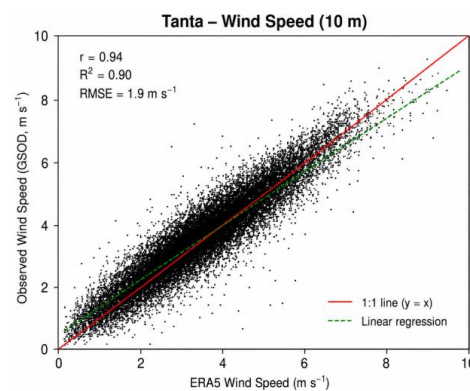
306

307

308

309

310



311

312

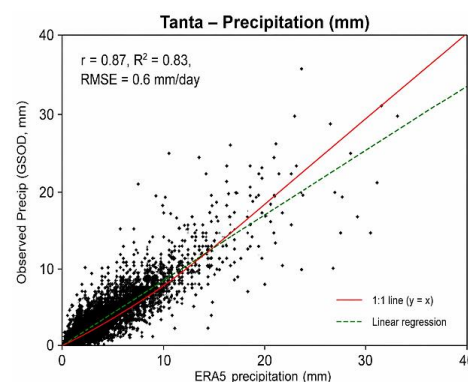
313

314

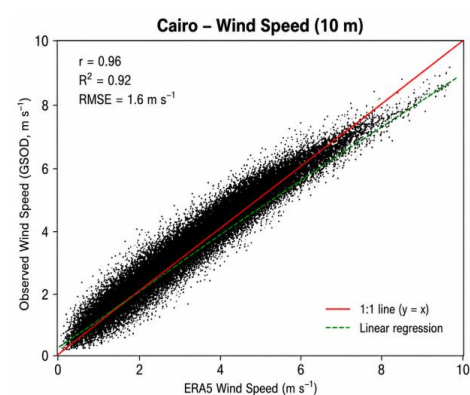
315

316

317



318



319

320

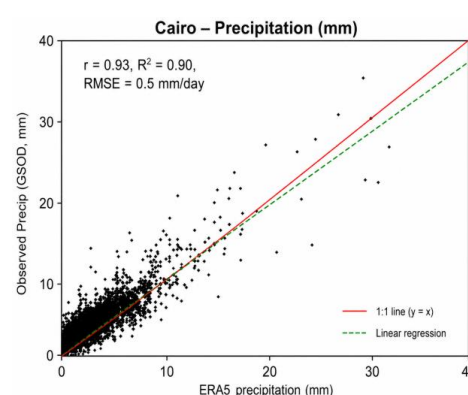
321

322

323

324

325



326

Figure 2. Scatterplots comparing ERA5 reanalysis data with daily surface observations extracted from the NOAA Global Surface Summary of the Day (GSOD) archive for wind speed (10 m) and precipitation at Alexandria, Tanta, and Cairo International Airport during 1980–2020. The solid red line denotes the 1:1 reference line ($y = x$), whereas the dashed green line represents the least-squares linear regression fitted to the observations.



331 These results indicate that ERA5 adequately reproduces the temporal variability of near-
332 surface wind speed and precipitation across the Nile Delta. The dataset therefore provides a
333 reliable basis for the subsequent climatological analysis of air stagnation patterns across the
334 region.

335 Air stagnation is operationally defined in this study following the meteorological criteria of
336 the NCDC Air Stagnation Index (ASI), which identifies stagnation days when three
337 atmospheric conditions occur simultaneously: weak near-surface winds, weak mid-
338 tropospheric flow, and the absence of precipitation (Horton and Harshvardhan, 2012; Huang
339 et al., 2017). A stagnation day occurs when surface wind speed is below 3.2 m s^{-1} , wind
340 speed at 500 hPa is below 13 m s^{-1} , and daily precipitation does not exceed 1 mm. Within
341 this framework, spatial variations in stagnation frequency are strongly linked to variability in
342 near-surface wind speed, particularly across low-relief continental plains where boundary-
343 layer ventilation is primarily regulated by horizontal wind intensity. The analyses presented
344 here therefore focus on the role of surface wind variability, while upper-level flow and
345 precipitation act as complementary constraints embedded within the stagnation index
346 formulation.

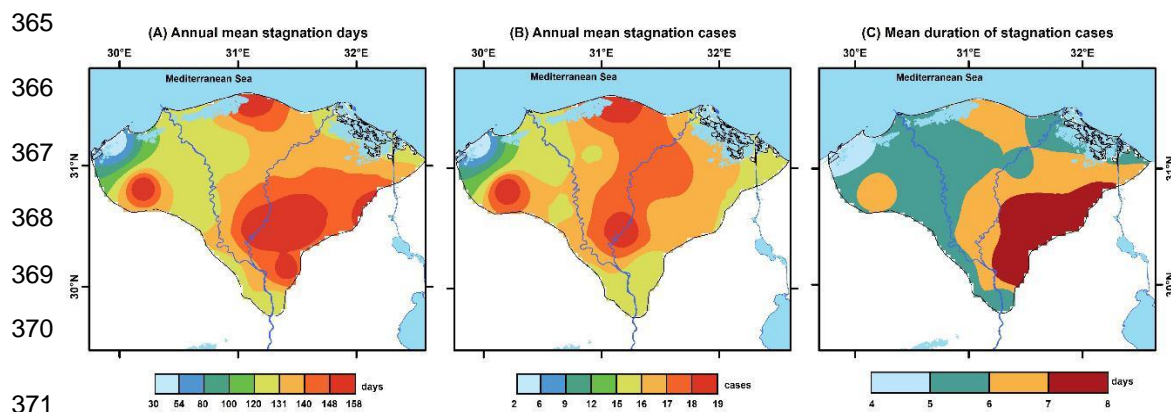
347 **4.1 Climatology and Spatial Patterns**

348 The spatial distribution of mean annual air stagnation days (Figure 3A) exhibits distinct
349 heterogeneity across the Egyptian Nile Delta. Central interior regions experience the highest
350 frequency, exceeding 150 days per year, whereas coastal zones, particularly in the northwest,
351 show lower frequencies, around 60 days annually. Mean annual stagnation cases (Figure 3B)
352 mirror this pattern, with more than 18 episodes per year clustered in the central Delta and
353 fewer than six in western and northern peripheries.

354 The mean duration of individual stagnation episodes (Figure 3C) ranges from 7–8 days in
355 central and eastern sectors, decreasing to less than 5 days along the coast. This spatial
356 gradient highlights the persistence of stagnant conditions in the Delta's interior, consistent
357 with limited near-surface ventilation. The convergence of high frequency and long-duration
358 zones defines recurrent stagnation hotspots, providing a robust depiction of spatial
359 climatology. these observations indicate that stagnation dynamics over the Nile Delta are
360 controlled primarily by local-scale ventilation efficiency and coastal influence, with interior
361 regions experiencing more prolonged and frequent stagnation. Together, these patterns



362 establish a coherent spatial climatology of air stagnation across the Nile Delta, characterized
363 by a maximum pronounced inland and a progressive decrease toward the Mediterranean
364 coast.

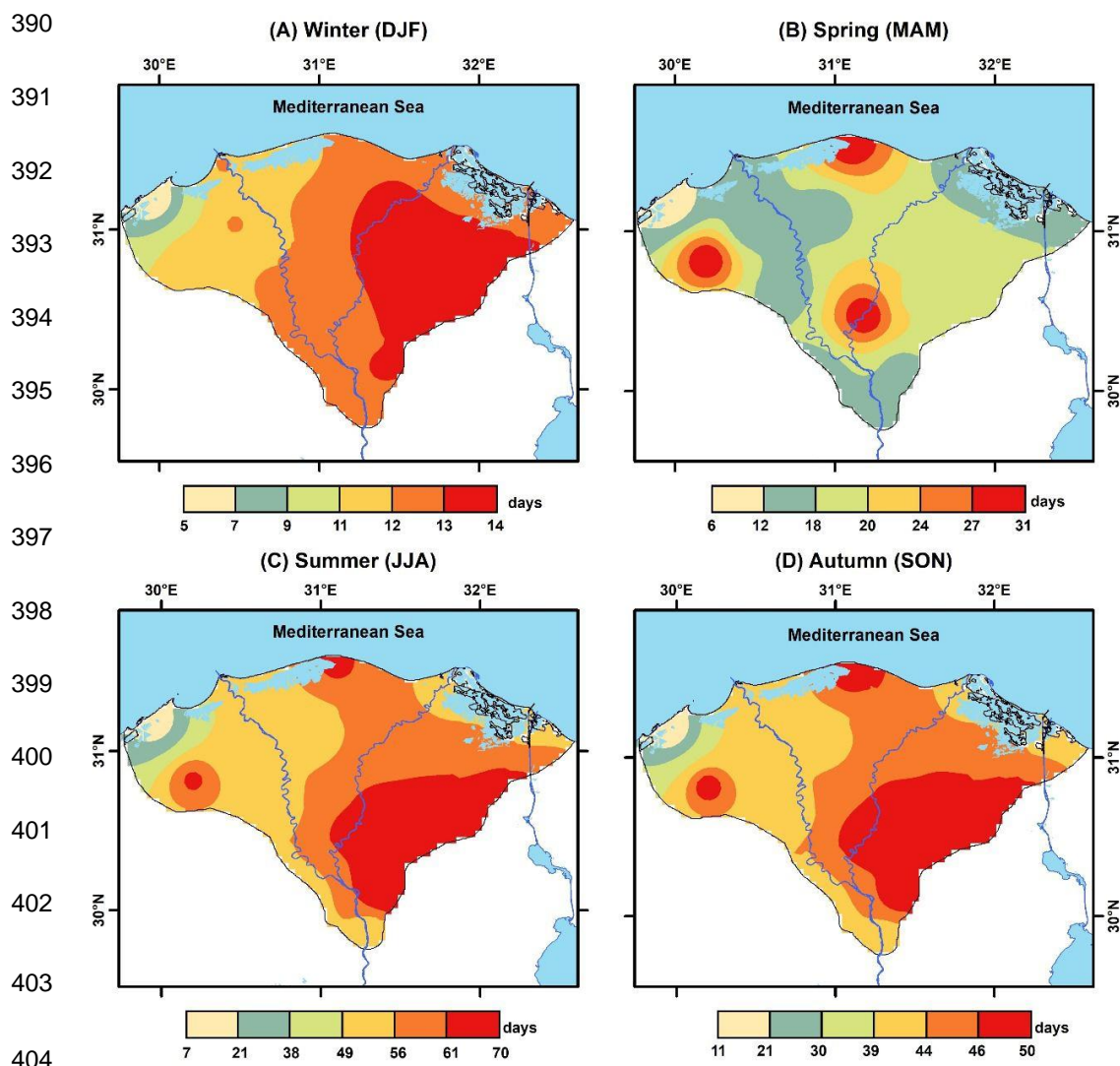


372 Figure 3 Spatial distribution of (a) mean annual air stagnation days, (b) mean annual
373 stagnation cases, and (c) mean duration of stagnation episodes (days) over the Egyptian Nile
374 Delta during 1980–2020.

375 4.2 Seasonal Dynamics

376 Figure 4 illustrates the seasonal distribution of mean air stagnation days across the Nile Delta
377 during 1980–2020. The spatial configuration reveals a pronounced annual cycle
378 characterized by a primary maximum in summer and a secondary peak in winter, while
379 spring and autumn exhibit comparatively lower frequencies.

380 In winter (DJF; Figure 4A), stagnation days are concentrated over the central and
381 northeastern sectors of the Delta, with seasonal totals generally ranging between 11 and 14
382 days. Coastal areas exhibit lower frequencies, reflecting the moderating influence of
383 maritime airflow. This spatial pattern is consistent with reduced surface wind speeds and
384 enhanced lower-tropospheric stability during periods dominated by anticyclonic conditions
385 over the eastern Mediterranean. Spring (MAM; Figure 4B) represents the minimum phase of
386 stagnation occurrence, with values generally remaining below 18 days across most of the
387 Delta. The spatial distribution becomes more fragmented, and only localized maxima persist
388 over interior areas. This decline coincides with strengthened westerly circulation and
389 enhanced horizontal mixing associated with transitional synoptic conditions.



405 Figure 4. Seasonal distribution of mean air stagnation days across the Nile Delta during
406 1980–2020 derived from ERA5 reanalysis data: (A) winter (DJF), (B) spring (MAM), (C)
407 summer (JJA), and (D) autumn (SON). Values represent the seasonal mean number of
408 stagnation days calculated according to the NCDC Air Stagnation Index criteria.

409 The highest stagnation frequencies occur during summer (JJA; Figure 4C). Seasonal totals
410 exceed 60 days across the central and southern Delta, indicating prolonged periods of weak
411 ventilation. This pattern corresponds with reduced sea–land pressure contrasts and the



412 seasonal intensification of the subtropical high over North Africa, conditions that Favour
413 weak surface winds ($U_{10} < 3.2 \text{ m s}^{-1}$) and increased boundary-layer stability. During autumn
414 (SON; Figure 4D), stagnation frequencies increase again to intermediate levels, typically
415 ranging between 30 and 45 days. The spatial pattern remains similar to that observed in
416 summer but with reduced intensity. This phase reflects the gradual transition from the
417 summer subsidence regime toward the more dynamically active winter circulation.

418 Overall, the seasonal distribution indicates that air stagnation across the Nile Delta is closely
419 linked to variations in surface wind intensity and boundary-layer stability associated with the
420 regional circulation cycle of the eastern Mediterranean.

421 **4.3 Temporal and Spatial Trends**

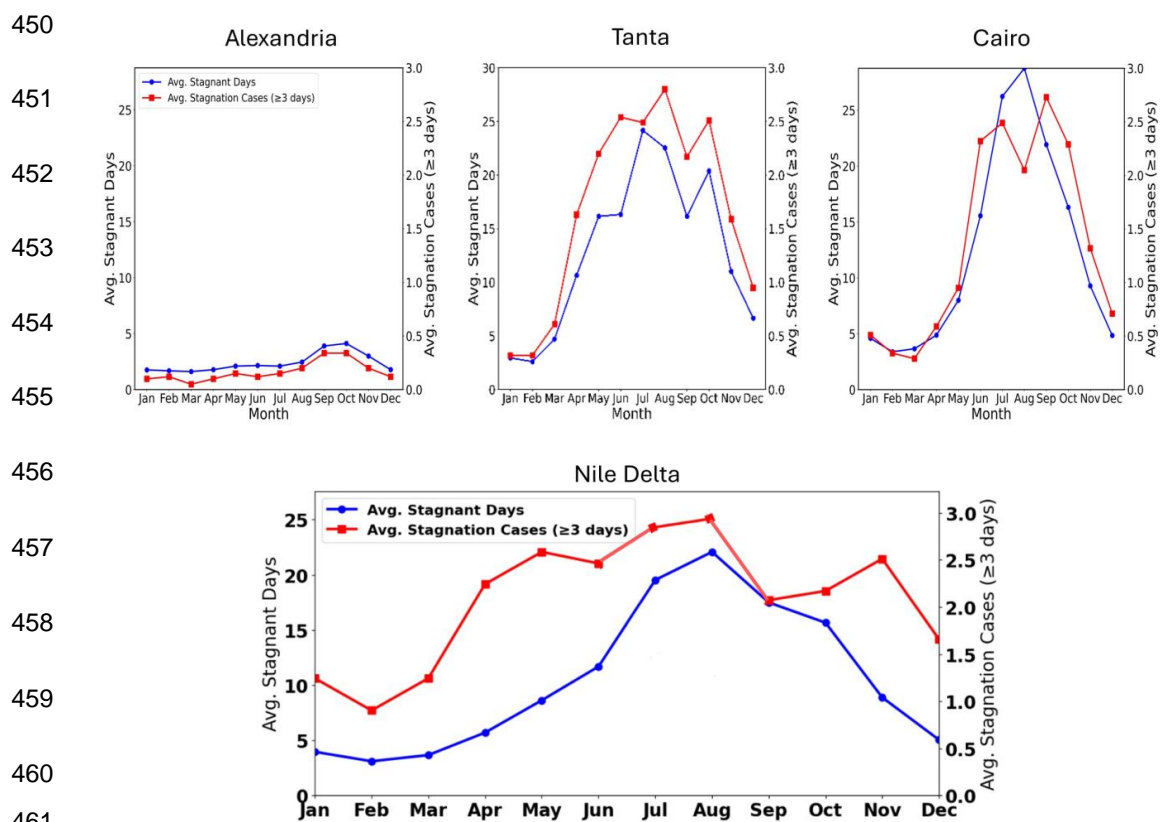
422 The examination of temporal and spatial trends in air stagnation provides a fundamental lens
423 through which the long-term behaviour of the atmospheric boundary layer over the Nile
424 Delta can be understood. Changes in the frequency and duration of stagnation episodes act as
425 sensitive diagnostics of dynamical and thermal transformations within the lower troposphere,
426 serving as indicators of variations in horizontal ventilation efficiency and thermal stability.
427 Accordingly, analysing these trends offers an integrated view of how the phenomenon has
428 evolved in magnitude and spatial structure across four consecutive decades, contributing to
429 the interpretation of emerging climatic imbalances within one of the most sensitive
430 Mediterranean environments to global climate change.

431 **4.3.1 Temporal Variability**

432 Figure 5 depicts a clear seasonal differentiation in the frequency of stagnation days and
433 episodes. Panel (a) shows that Alexandria, the coastal station most directly influenced by the
434 maritime boundary layer, exhibits the lowest exposure to stagnation, with monthly averages
435 rarely exceeding four days and a standard deviation of ± 1.5 days. This limited variability
436 underscores the regulating influence of the Mediterranean Sea–land breeze circulation, which
437 continuously renews the near-surface air and enhances mechanical dispersion, preventing
438 prolonged atmospheric confinement. Panel (b), representing Tanta in the central Delta,
439 reveals a gradual rise in the number of stagnation days beginning in April and peaking in
440 July, with monthly means approaching 26 days and a standard deviation near ± 2.8 days. This
441 escalation mirrors the seasonal transition from maritime to inland thermodynamic control,
442 reflecting the progressive dominance of synoptic subsidence and reduced ventilation



443 efficiency across the Delta’s interior. Panel (c) portrays Cairo, the most continental of the
 444 Delta stations, recording the highest stagnation frequency, exceeding 28 days per month
 445 during summer. This extreme persistence indicates a near-complete decoupling of the
 446 planetary boundary layer from the free atmosphere, accompanied by the establishment of a
 447 robust thermodynamic stability regime over the urban heat island. Such persistent
 448 stratification confines air masses and extends pollutant residence time, effectively
 449 transforming Cairo into a semi-permanent atmospheric sink during peak summer months.



462 Figure 5. Monthly evolution of air stagnation days and prolonged stagnation episodes (≥ 3
 463 consecutive days) across three representative Nile Delta stations (Alexandria, Tanta, and Cairo)
 464 derived from surface and radiosonde observations, alongside the Delta-wide climatological mean
 465 reconstructed from ERA5 reanalysis for 1980–2020.

466 Across all three stations, the parallel seasonal evolution of the curves in Figure 5 indicates
 467 that the increase in stagnation days primarily results from the lengthening of individual



468 stagnation events, rather than a higher count of short-lived episodes. This persistence-
469 oriented character is typical of broad alluvial plains, where seasonal continuity of stagnation
470 episodes is amplified by the weak dynamic forcing and subdued synoptic modulation.

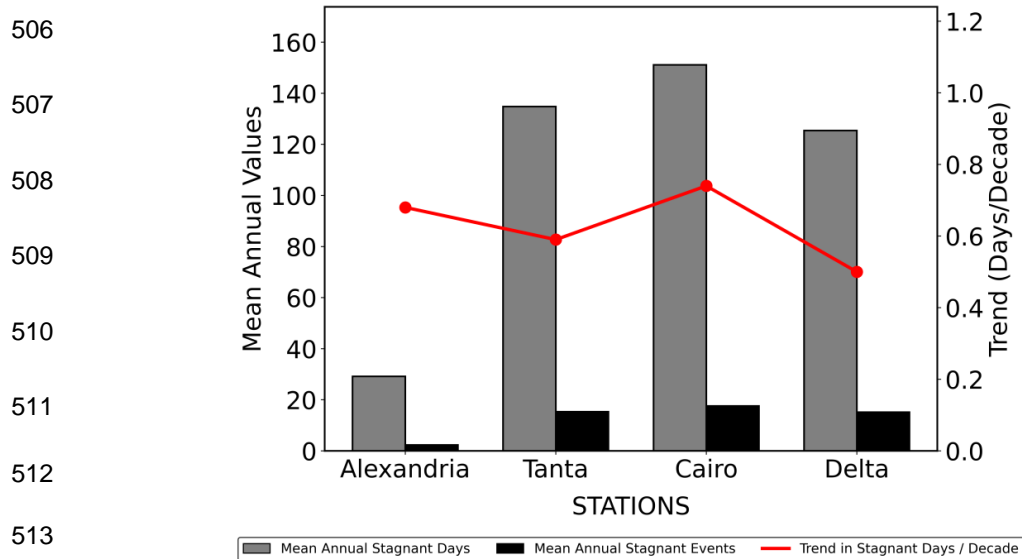
471 To determine whether this local signal represents a regionally coherent pattern, panel (d)
472 presents the Delta-wide average derived from ERA5 reanalysis data. The regional trend
473 exhibits a steady increase in mean stagnation days from April to the summer apex (July–
474 August), surpassing 20 days per month. The close alignment between the regional curves for
475 stagnation days and events confirms that the observed intensification reflects longer-lasting
476 stagnation episodes rather than episodic multiplicity. This correspondence highlights the
477 structural dominance of persistent atmospheric stillness, a hallmark of semi-arid
478 Mediterranean stagnation regimes.

479 Consistent with global studies of stagnation-prone environments in the Mediterranean and
480 subtropical domains, such as those reported by Horton et al. (2012) and Huang et al. (2018),
481 the seasonal peak is linked to diminished upper-level synoptic activity and weakened surface
482 pressure gradients. The temporal behaviour observed here can be attributed to the
483 predominance of quasi-stationary pressure systems during summer, particularly the
484 northward extension of the Sudan Low combined with the decline of upper-level westerly
485 activity. These features jointly suppress horizontal ventilation and foster the accumulation of
486 warm air masses near the surface. Conversely, during winter, increased Mediterranean
487 cyclonic activity and frequent frontal passages invigorate surface winds and enhance air-
488 mass renewal, leading to a sharp reduction in stagnation frequency.

489 Taken together, these findings delineate a pronounced spatial gradient in stagnation intensity
490 across the Nile Delta, increasing southward from the maritime to the continental interior.
491 This gradient encapsulates the atmospheric transition from a ventilated maritime regime to a
492 quiescent continental regime, defining the dynamic nucleus of the spatial tendencies explored
493 in the subsequent section. From a climatic perspective, this progressive intensification
494 signifies the Delta's transformation into a sensitive atmospheric basin where thermal forcing,
495 synoptic modulation, and anthropogenic surface heating converge to regulate boundary-layer
496 behaviour. Collectively, the temporal signals portrayed here reveal not only a seasonal
497 oscillation but also an emerging climatological reconfiguration of the eastern Mediterranean
498 boundary-layer system under regional warming pressures.



499 Figure 6 summarizes the long-term evolution of air stagnation across the coastal–inland
 500 gradient of the Nile Delta using three representative stations together with the Delta-wide
 501 mean derived from ERA5. Trend magnitudes were estimated using Sen's slope estimator,
 502 whereas statistical significance was evaluated with the Mann–Kendall test after correcting
 503 for serial autocorrelation following Hamed and Rao (1998). Overall, the results reveal a
 504 consistent positive trend in stagnation frequency across all locations, although the magnitude
 505 of the increase varies along the coastal–inland gradient.



514 Figure 6. Mean annual air stagnation days, prolonged stagnation episodes, and decadal trends
 515 across three representative stations (Alexandria, Tanta, and Cairo Airport) together with the
 516 Delta-wide mean derived from ERA5 reanalysis (1980–2020). Grey bars denote the mean annual
 517 number of stagnation days, black bars indicate the mean annual number of prolonged stagnation
 518 episodes, and the red line represents the corresponding Sen's slope trend estimates (days
 519 decade⁻¹). Trend significance was evaluated using the Mann–Kendall test after correction for
 520 serial autocorrelation.

521 Alexandria exhibits the lowest annual stagnation frequency (approximately 30 days yr⁻¹)
 522 together with a modest positive trend of about +0.67 days decade⁻¹, reflecting the persistent
 523 ventilating influence of the Mediterranean. Stagnation becomes progressively more frequent
 524 inland, with Tanta recording approximately 135 days yr⁻¹ and a positive trend of about +0.60
 525 days decade⁻¹. Cairo displays the highest annual stagnation frequency (approximately 150
 526 days yr⁻¹) and the strongest increase (about +0.73 days decade⁻¹), whereas the Delta-wide



527 mean reaches approximately 125 stagnation days yr^{-1} with a comparatively weaker positive
528 trend of about $+0.50$ days decade^{-1} .

529 The close correspondence between mean stagnation frequency, prolonged stagnation
530 episodes, and the positive Sen's slope estimates indicates that the observed increase primarily
531 reflects a gradual intensification of persistent stagnation conditions rather than a greater
532 occurrence of isolated short-lived events. Taken together, Figure 6 depicts a coherent long-
533 term strengthening of atmospheric stagnation across the Nile Delta while preserving the
534 pronounced coastal–inland gradient evident throughout the analysis. This spatial pattern is
535 consistent with progressively weaker ventilation from the Mediterranean coast toward the
536 continental interior, reinforcing the climatological interpretation developed in the preceding
537 sections.

538 **4.3.2 Spatial Trends**

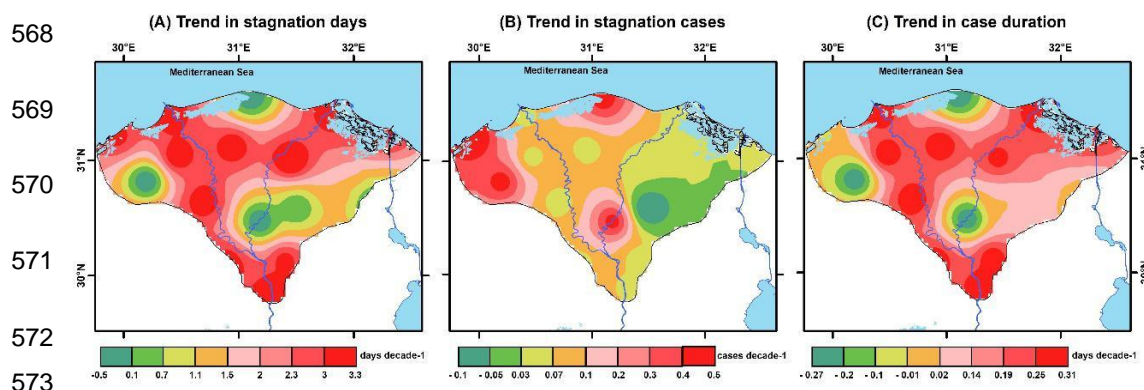
539 Spatial patterns of long-term trends in air stagnation metrics across the Nile Delta are
540 presented in Figure 7. Trends were calculated for each ERA5 grid cell using Sen's slope
541 estimator, while statistical significance was evaluated using the Mann–Kendall test as
542 described in Section 3.5. The resulting maps therefore illustrate the spatial magnitude of
543 decadal changes in stagnation characteristics during the period 1980–2020.

544 Panel (a) displays the spatial distribution of trends in the annual number of stagnation days.
545 Positive trends dominate most of the Delta, with magnitudes ranging from approximately
546 $+0.5$ to $+3.3$ days per decade. The strongest increases occur across the central and southern
547 sectors of the Delta, particularly along the Tanta–El-Mahalla and Banha–Mansoura corridors,
548 indicating a gradual intensification of stagnation frequency within the inland portions of the
549 region. In contrast, weaker trends appear along the northwestern coastal fringe, where the
550 persistent influence of Mediterranean maritime ventilation moderates the long-term growth
551 of stagnation conditions. Panel (b) illustrates the spatial trends in the number of stagnation
552 events. The pattern broadly resembles that observed for stagnation days, although the
553 magnitude of change is smaller, ranging between approximately $+0.05$ and $+0.4$ events per
554 decade. Localized clusters of increasing event frequency emerge across central Delta sectors
555 and parts of the western coastal transition zone near Alexandria and Kafr El-Dawar. These
556 patterns indicate that the observed increase in stagnation days partly reflects a growing
557 recurrence of stagnation episodes across inland areas. Panel (c) presents trends in the mean
558 duration of stagnation events. Most grid cells exhibit weak to moderate positive tendencies,



559 typically between +0.1 and +0.3 days per decade, suggesting a gradual extension in the
 560 persistence of individual stagnation episodes. In contrast, parts of the eastern coastal sector
 561 show slight negative slopes (up to -0.2 days per decade), indicating shorter event durations
 562 in areas more directly influenced by coastal airflow.

563 Taken together, the three panels in Figure 7 indicate that the observed increase in stagnation
 564 days across much of the Nile Delta reflects the combined effect of moderately increasing
 565 event frequency and a gradual extension of event persistence, particularly across inland
 566 sectors. The spatial coherence of these patterns highlights the inland sectors of the Delta as
 567 the primary centers of stagnation intensification over the past four decades.



574 Figure 7. Spatial distribution of decadal trends in (a) the number of air stagnation days, (b)
 575 the frequency of stagnation events, and (c) the mean duration per event across the Nile Delta
 576 during 1980–2020.

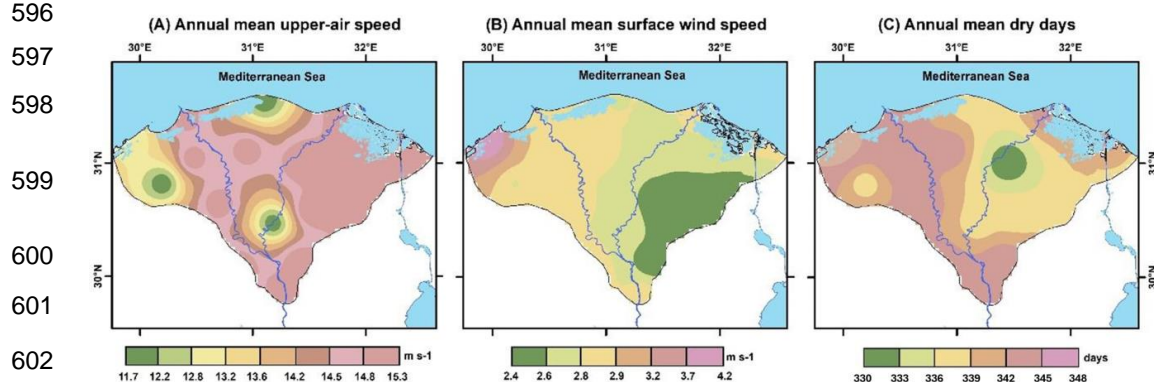
577 4.3.3 Atmospheric Dynamics and Stagnation

578 Figure 8 illustrates the spatial configuration of key atmospheric variables associated with air
 579 stagnation across the Nile Delta during 1980–2020, including upper-level wind speed (500
 580 hPa), near-surface wind speed (10 m), and the annual frequency of dry days. These variables
 581 correspond directly to the principal components of the Air Stagnation Index and provide a
 582 dynamical context for interpreting the spatial distribution of stagnation conditions.

583 In panel (a), mean wind speeds at 500 hPa range between 11.7 and 15.3 m s^{-1} , with relatively
 584 weaker values across the central and southern sectors of the Delta and stronger flow toward
 585 the northwestern margin. This spatial gradient indicates a modest reduction in upper-level
 586 flow intensity over the interior of the Delta compared with the coastal sector. Panel (b)
 587 presents the distribution of near-surface wind speeds, which vary between 2.4 and 4.7 m s^{-1} .



588 The lowest velocities occur primarily over the eastern and south-central Delta, while higher
589 wind speeds are observed toward the Mediterranean coastline. These contrasts highlight the
590 inland weakening of low-level ventilation relative to the more dynamically active coastal
591 zone influenced by maritime airflow. Panel (c) shows the spatial distribution of annual dry-
592 day frequency, ranging from approximately 330 to 348 days yr⁻¹. The highest values are
593 concentrated across the central and southeastern Delta, whereas relatively lower frequencies
594 occur along the northwestern coastal sector.
595
596



603 Figure 8. Spatial distribution of mean wind speed at 500 hPa (a), surface wind speed (b), and
604 number of dry days (c) across the Nile Delta during 1980–2020.

605 A comparison of the three panels reveals a consistent spatial correspondence: regions
606 characterized by weaker upper-level and surface winds generally coincide with areas
607 experiencing higher frequencies of dry days. This configuration reflects the co-occurrence of
608 reduced horizontal ventilation and limited precipitation across the Delta's interior, conditions
609 that favor the development and persistence of air stagnation.

610 Taken together, these spatial patterns indicate that the interior sectors of the Nile Delta
611 experience a combination of weaker atmospheric flow and prolonged dry conditions relative
612 to the coastal margin. Such a configuration provides a dynamical setting conducive to
613 stagnation persistence within the regional boundary-layer environment.

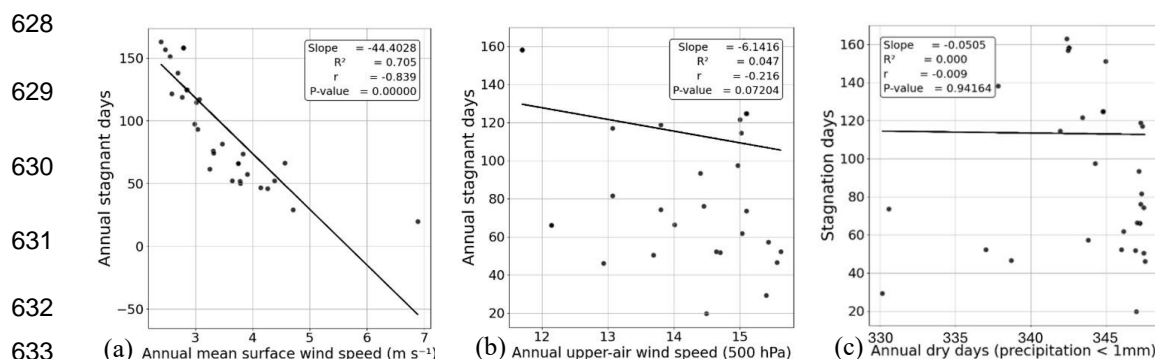
614 4.3.4 Statistical Relationships with Atmospheric Variables

615 To clarify the atmospheric mechanisms underlying the spatial distribution of stagnation
616 across the Nile Delta, statistical relationships between stagnation frequency and key
617 atmospheric variables were examined. Because the analysis is based on spatial grid cells



618 derived from a continuous atmospheric field, neighboring cells may exhibit spatial
 619 dependence. Consequently, the reported correlation statistics should be interpreted as
 620 indicative of regional associations rather than strictly independent statistical relationships.

621 Figure 9 illustrates the spatial relationships between mean annual air stagnation frequency
 622 and three key atmospheric controls across the Nile Delta: near-surface wind speed (10 m),
 623 upper-level wind speed at 500 hPa, and the annual number of dry days. Because the analysis
 624 is conducted on spatial grid cells derived from a continuous atmospheric field, neighbouring
 625 cells may not be fully independent and can exhibit a degree of spatial autocorrelation.
 626 Consequently, the reported correlation statistics should be interpreted as indicative of
 627 regional associations rather than strictly independent statistical relationships.



634 Figure 9. Spatial statistical relationships between mean annual air stagnation frequency and key
 635 atmospheric controls across the Nile Delta during 1980–2020. Panels illustrate correlations with
 636 (a) mean surface wind speed (10 m), (b) upper-level wind speed at 500 hPa, and (c) annual
 637 number of dry days (precipitation < 1 mm). Each point represents an ERA5 grid cell within the
 638 study domain.

639 Panel (a) shows a strong and statistically significant inverse correlation between air
 640 stagnation frequency and mean surface wind speed ($r = -0.839$, $R^2 = 0.705$, $p < 0.001$). The
 641 number of stagnation days decreases by approximately 44 days for every 1 m s^{-1} increase in
 642 near-surface wind velocity. This relationship also reflects the broader climatological control
 643 exerted by near-surface wind regimes on atmospheric ventilation across the Delta, beyond
 644 the threshold condition embedded within the stagnation index. This robust negative
 645 relationship highlights the decisive role of horizontal ventilation in disrupting stagnation
 646 events and weakening the stable boundary layer over the Delta’s flat alluvial plains. It also



647 demonstrates the sensitivity of the local microclimate to minor variations in surface wind
648 intensity, where small perturbations in low-level flow can markedly influence stagnation
649 persistence and duration.

650 Panel (b) reveals a weak and statistically insignificant association between stagnation
651 frequency and upper-tropospheric wind speed at 500 hPa ($r = -0.216$, $R^2 = 0.047$, $p = 0.07$).
652 This suggests that variability in free-atmospheric circulation does not directly affect
653 boundary-layer dynamics near the surface. The pattern reflects a pronounced boundary-layer
654 decoupling regime that restricts the downward transfer of synoptic momentum and limits
655 vertical ventilation efficiency. Such behavior agrees with findings reported by Horton et al.
656 (2012) and Huang et al. (2017), who observed that stagnation in semi-continental settings is
657 essentially a near-surface phenomenon driven by thermal stability and weak turbulent mixing
658 rather than large-scale synoptic forcing.

659 Panel (c) shows no statistically significant correlation between stagnation frequency and the
660 number of dry days ($r \approx 0$). This implies that variations in surface humidity or the frequency
661 of non-precipitating days do not play a major role in determining stagnation behavior over
662 the Nile Delta. The phenomenon arises primarily from the interaction between weak
663 horizontal ventilation and enhanced dynamic–thermal stability; a ventilation–stability
664 coupling that sustains prolonged stagnation episodes and increases the susceptibility of the
665 local climatic system to seasonal-scale fluctuations.

666 Taken together, these relationships highlight the dominant role of near-surface wind
667 dynamics in regulating air stagnation across the Nile Delta. The strong sensitivity of
668 stagnation frequency to surface wind speed indicates that small variations in horizontal
669 ventilation can substantially alter boundary-layer renewal over the Delta’s flat alluvial
670 terrain. In contrast, the weak association with upper-level winds and dry-day frequency
671 suggests that stagnation persistence is primarily governed by local boundary-layer stability
672 rather than by variability in free-tropospheric circulation or moisture conditions. These
673 results emphasize that atmospheric ventilation efficiency represents the principal physical
674 control on stagnation behavior in the region.

675 **5 Discussion**

676 The results indicate that atmospheric stagnation over the Nile Delta constitutes a persistent
677 climatic feature rather than an episodic meteorological anomaly. The spatial and temporal



678 organization of stagnation identified in this study suggests that the Nile Delta functions as a
679 dynamically coherent stagnation regime, where weak horizontal ventilation and persistent
680 boundary-layer stability jointly regulate atmospheric renewal across the region. Similar
681 dynamical configurations have been documented in other stagnation-prone environments,
682 where reduced near-surface ventilation and enhanced lower-tropospheric stability promote
683 the persistence of stagnant air masses (Horton et al., 2012; Huang et al., 2017; Huang et al.,
684 2018). The stagnation thresholds applied in this study follow the classical Air Stagnation
685 Index formulation proposed by Wang and Angell (1999) and widely adopted in subsequent
686 climatological investigations (e.g., Horton et al., 2012; Huang et al., 2018). Employing the
687 same criteria ensures methodological consistency and enables direct comparison between the
688 stagnation characteristics observed over the Nile Delta and those reported for other regional
689 and global environments. Within this regime, reduced horizontal ventilation, relatively weak
690 upper-tropospheric flow, and enhanced thermal stability within the planetary boundary layer
691 jointly favor the development of prolonged stagnation episodes. These characteristics suggest
692 that stagnation across the Delta reflects broader circulation conditions that limit atmospheric
693 ventilation efficiency rather than isolated local events.

694 The spatial and seasonal coherence of stagnation patterns further indicates that the
695 phenomenon is embedded within the regional circulation regime of the eastern
696 Mediterranean. In particular, the persistence of stagnation conditions appears to be linked to
697 a gradual reduction in thermal and pressure gradients between the Mediterranean Sea and the
698 adjacent continental interior. This reduction is consistent with the northward expansion of the
699 subtropical anticyclone during summer reported in previous studies of the eastern
700 Mediterranean, a circulation configuration that suppresses synoptic variability and promotes
701 stable atmospheric conditions. From a dynamical perspective, these conditions favor
702 enhanced lower-tropospheric stability and reduced boundary-layer ventilation efficiency.
703 Comparable tendencies toward increased atmospheric stability have been reported across the
704 eastern Mediterranean basin under recent warming conditions (Seidel et al., 2008; Huang et
705 al., 2018).

706 Spatially, the annual distribution of stagnation days reveals a pronounced inland core
707 extending across the central and southern sectors of the Nile Delta, where annual totals
708 exceed 150 days. In contrast, coastal locations such as Alexandria experience substantially
709 fewer events, averaging approximately 60 stagnation days per year, reflecting the moderating



710 influence of persistent sea-breeze circulation and marine air ventilation. This pronounced
711 coastal–inland gradient indicates a progressive reduction in ventilation efficiency from the
712 Mediterranean shoreline toward the interior Delta plains. Under such conditions, weak
713 vertical wind shear and reduced turbulent mixing within the planetary boundary layer limit
714 vertical air exchange and promote the near-surface accumulation of heat, aerosols, and
715 pollutants. The resulting thermally stratified structure enhances atmospheric stability and
716 prolongs stagnation persistence. Similar spatial configurations have been reported in other
717 low-relief coastal–continental transition environments, including the North China Plain and
718 parts of the southern United States (Horton et al., 2012; Huang et al., 2017).

719 The seasonal cycle of stagnation exhibits a pronounced summer maximum and a secondary
720 winter peak, separated by lower frequencies during the transitional seasons of spring and
721 autumn. Summer conditions dominate the annual stagnation regime under the influence of
722 the expanded subtropical high, when surface wind speeds frequently fall below 3.2 m s^{-1} and
723 nocturnal temperature inversions become more persistent. These conditions promote
724 enhanced decoupling within the planetary boundary layer, particularly over Cairo and the
725 southern sectors of the Delta, where stagnation persists for more than 150 days annually. The
726 weak statistical relationship between stagnation frequency and upper-level wind speed ($r =$
727 -0.216) suggests that stagnation variability is primarily governed by lower-tropospheric
728 processes rather than large-scale synoptic flow. Similar seasonal behavior has been
729 documented in semi-arid regions of East Asia and the Mediterranean, where reduced near-
730 surface ventilation and stable boundary-layer conditions promote prolonged stagnation
731 events (Horton et al., 2012; Li et al., 2021).

732 Over the four-decade observational period, the temporal evolution indicates a gradual
733 increase in both the frequency and persistence of stagnation events, averaging approximately
734 0.6 day per decade. Across inland sectors of the Delta, summer contributes more than half of
735 the annual stagnation total, with seasonal averages exceeding sixty days. This pronounced
736 seasonal concentration implies that the long-term increase in annual stagnation frequency is
737 largely driven by changes occurring during the warm season. The dominance of summer
738 stagnation suggests that persistent subsidence and sustained reductions in near-surface wind
739 speeds during this period provide the primary dynamical context for the observed long-term
740 increase in stagnation occurrence.



741 The intensification of stagnation is consistent with the broader decline in near-surface wind
742 speeds documented across the Mediterranean and other subtropical regions during recent
743 decades (Vautard et al., 2010; McVicar et al., 2012; Azorin-Molina et al., 2019). Across the
744 Nile Delta, stagnation frequency exhibits a remarkably strong inverse association with near-
745 surface wind speed ($r = -0.839$), underscoring the pivotal role of horizontal ventilation in
746 regulating boundary-layer renewal. This relationship indicates that even modest reductions in
747 surface wind intensity can substantially suppress atmospheric mixing and prolong stagnation
748 conditions across the Delta's low-relief alluvial landscape. Under weak-wind conditions,
749 reduced momentum transfer suppresses turbulent mixing within the planetary boundary layer
750 and slows the renewal of near-surface air masses, allowing thermally stable conditions to
751 persist for extended periods. Comparable mechanisms have been documented in other
752 stagnation-prone regions where declining wind speeds increase atmospheric residence times
753 and promote pollutant accumulation (Vautard et al., 2010; Horton et al., 2012; Huang et al.,
754 2017).

755 This dynamical configuration reflects a close coupling between horizontal ventilation and
756 thermal stability within the boundary layer. When surface and upper-level winds weaken
757 under persistently dry and radiatively intense conditions, vertical turbulence is suppressed.
758 Under such circumstances, the lower atmosphere may evolve toward a quasi-isolated
759 boundary-layer system. Within this environment, dry-day frequency may reach up to 348
760 days per year in some sectors of the Delta, indicating extremely limited moisture availability
761 and reduced convective potential. Similar mechanisms have been reported in semi-arid
762 regions where widespread wind stilling contributes directly to the persistence of atmospheric
763 stagnation (Horton et al., 2012; Vautard et al., 2010).

764 In a broader context, the stagnation characteristics of the Nile Delta share several similarities
765 with major global stagnation hotspots such as the Beijing–Tianjin Basin and the Los Angeles
766 Basin (Horton et al., 2014; Tai et al., 2012). However, the underlying mechanisms differ
767 substantially. Whereas those regions are strongly influenced by orographic confinement,
768 stagnation over the Nile Delta likely develops under quasi-stationary pressure and thermal
769 configurations across a nearly flat terrain. The absence of significant topographic enclosure
770 indicates that stagnation persistence in the region is governed primarily by dynamical and
771 thermodynamic controls rather than geometric basin effects.



772 The environmental implications of this stagnation regime may be significant. Persistent
773 stagnation across the central Delta, combined with rapid urban expansion, promotes a local
774 atmospheric environment characterized by reduced air-mass exchange and limited heat
775 dispersion. Under such conditions, the accumulation of fine particulate matter (PM_{2.5}) and
776 ozone (O₃) frequently exceeds World Health Organization guideline levels, particularly
777 across Greater Cairo (Hereher et al., 2022). These elevated pollutant concentrations coincide
778 spatially with urban heat-island centers and major emission sources, creating reinforcing
779 feedbacks in which urbanization enhances thermal stability through anthropogenic heat
780 release and surface sealing, while stagnation simultaneously increases pollutant residence
781 time and heat stress. Comparable feedback mechanisms have been documented in other
782 urbanized stagnation regions such as the Los Angeles and Beijing–Tianjin basins (Horton et
783 al., 2014; Cerro et al., 2015).

784 The sustained increase in stagnation frequency therefore suggests a gradual shift in the
785 lower-tropospheric balance between horizontal ventilation and atmospheric stability across
786 the Nile Delta. From a climatic perspective, These conditions are consistent with previously
787 reported circulation adjustments across the eastern Mediterranean, including the increasing
788 persistence of subtropical high-pressure systems and reduced synoptic variability during
789 summer (Seidel et al., 2008; Hu et al., 2013; Azorin-Molina et al., 2019). Although the
790 present analysis does not explicitly quantify long-term trends in geopotential height or
791 pressure gradients, incorporating such diagnostics in future work would help clarify the
792 dynamical linkage between stagnation variability and regional circulation changes.

793 Within this evolving atmospheric context, understanding stagnation dynamics is important
794 not only for climatological assessment but also for environmental management. The
795 integration of stagnation indicators into air-quality monitoring systems and urban planning
796 strategies in Egypt may therefore become increasingly valuable. Predictive modeling
797 frameworks that combine climatic observations, boundary-layer dynamics, and urban land-
798 surface processes will be particularly important for assessing how the Nile Delta may
799 respond to continued warming and rapid urbanization.

800 Taken together, these findings suggest that the Nile Delta represents a coastal plain
801 increasingly prone to atmospheric stagnation. where declining near-surface ventilation and
802 increasing boundary-layer stability interact to reshape the regional atmospheric renewal



803 regime. Similar tendencies have been reported across several subtropical and Mediterranean
804 environments experiencing widespread reductions in surface wind speeds and enhanced
805 atmospheric stability under recent climate warming (Vautard et al., 2010; McVicar et al.,
806 2012; Azorin-Molina et al., 2019).

807 **6 Study Limitations**

808 Despite the robustness of the analytical framework adopted in this study, several
809 methodological and physical constraints should be acknowledged to properly contextualize
810 the interpretation of the results.

811 The first limitation relates to the intrinsic characteristics of the ERA5 reanalysis dataset used
812 in the analysis. Although ERA5 provides a dynamically consistent reconstruction of large-
813 scale atmospheric circulation and synoptic variability (Hersbach et al., 2020), its spatial
814 resolution remains insufficient to fully resolve mesoscale processes operating along the
815 complex land–sea interface of the northern Nile Delta. Coastal boundary-layer processes
816 such as sea-breeze circulations and local convergence zones may not be explicitly
817 represented within the reanalysis grid. Consequently, small-scale variations in near-surface
818 ventilation may be partially smoothed in coastal sectors, introducing a degree of uncertainty
819 in the diagnosis of stagnation frequency near the Mediterranean shoreline.

820 A second limitation concerns the set of atmospheric variables included in the stagnation
821 framework. The analysis was intentionally restricted to the core dynamical components of
822 the classical Air Stagnation Index, namely surface wind speed, mid-tropospheric wind speed,
823 and precipitation, following the methodology proposed by Wang and Angell (1999) and
824 Horton et al. (2012). While this approach ensures comparability with previous climatological
825 studies, it does not explicitly incorporate thermodynamic variables such as planetary
826 boundary-layer height (PBLH) or surface turbulent heat fluxes. These parameters have been
827 shown to modulate boundary-layer stability and may influence the intensity and persistence
828 of stagnation episodes in arid and semi-arid environments (Zittis et al., 2021; Zhou et al.,
829 2024).

830 A third limitation arises from the limited spatial density of long-term meteorological
831 observations available for validation across the Nile Delta. Although three representative
832 stations were used to evaluate the consistency of ERA5 surface fields, the existing
833 observational network remains sparse relative to the pronounced urban–rural and coastal–



834 inland gradients characterizing the region. A denser observational infrastructure would allow
835 a more detailed assessment of local ventilation regimes and would improve the calibration of
836 reanalysis-based diagnostics.

837 Finally, the present study adopts a diagnostic climatological approach based on historical
838 reanalysis data rather than employing high-resolution regional climate modelling or future
839 emission scenarios. As a result, the analysis primarily characterizes the recent climatological
840 baseline of stagnation conditions over the Nile Delta rather than their potential future
841 evolution under projected climate change.

842 Notwithstanding these limitations, the multi-decadal coverage of the dataset, combined with
843 the spatially explicit grid-cell analysis and the integration of observational validation,
844 provides a coherent empirical framework for understanding the climatology and recent
845 evolution of air stagnation across the Nile Delta. The results therefore offer a valuable
846 reference baseline for future studies seeking to explore the dynamical drivers and potential
847 future trajectories of atmospheric stagnation in rapidly urbanizing coastal lowlands.

848 **7 Uncertainty Assessment**

849 Uncertainty in the present analysis arises from three principal sources: the characteristics of
850 the reanalysis dataset, the operational thresholds used to diagnose stagnation, and the spatial–
851 temporal aggregation of the atmospheric fields. Recognizing these factors is essential for
852 interpreting the robustness of the derived stagnation climatology over the Nile Delta.

853 The first source of uncertainty is associated with the use of reanalysis products. ERA5 and
854 ERA5-Land provide dynamically consistent atmospheric reconstructions generated by the
855 ECMWF Integrated Forecasting System; however, reanalysis fields remain model-
856 constrained estimates whose accuracy depends on the density and distribution of assimilated
857 observations (Hersbach et al., 2020). This limitation is particularly relevant for near-surface
858 wind fields in low-relief coastal environments where observational coverage remains uneven.
859 Across parts of the Nile Delta, the relatively sparse distribution of meteorological stations
860 may introduce localized uncertainty in the representation of weak-wind conditions that are
861 critical for diagnosing stagnation events.

862 A second source of uncertainty relates to the thresholds used to identify stagnation
863 conditions. The criteria adopted in this study, namely surface wind speed $< 3.2 \text{ m s}^{-1}$, mid-



864 tropospheric wind speed at 500 hPa $< 13 \text{ m s}^{-1}$, and daily precipitation $< 1 \text{ mm day}^{-1}$, follow
865 the classical Air Stagnation Index formulation widely applied in climatological analyses
866 (Horton et al., 2014; Huang et al., 2017). Sensitivity tests indicate that moderate threshold
867 adjustments ($\pm 10 \%$) modify the estimated annual stagnation frequency by less than 5 %,
868 suggesting that the diagnosed spatial and temporal patterns remain relatively insensitive to
869 small variations in the operational definition.

870 Temporal aggregation introduces an additional, though limited, source of uncertainty. Hourly
871 ERA5 outputs were aggregated to daily means in order to maintain consistency with the
872 stagnation index formulation. This procedure may smooth short-lived sub-daily variability,
873 particularly during transitional seasons when boundary-layer coupling varies on diurnal time
874 scales. Nevertheless, comparisons across daily, monthly, and seasonal aggregations reveal
875 consistent spatial structures and temporal signals, indicating that aggregation effects do not
876 materially alter the climatological patterns identified in this study.

877 Spatial resolution represents a further source of uncertainty. The $0.25^\circ \times 0.25^\circ$ ERA5 grid is
878 appropriate for regional-scale climatological analysis but cannot fully resolve fine-scale
879 heterogeneity associated with urban land cover, irrigation patterns, or localized coastal
880 circulations. Similar limitations have been documented in other low-relief deltaic
881 environments where boundary-layer processes operate at spatial scales smaller than those
882 represented in global reanalysis datasets (Huang et al., 2018).

883 Taken together, these factors primarily affect the precise magnitude of stagnation estimates
884 rather than the overall spatial distribution or long-term variability reported here. The
885 consistency between sensitivity analyses, validation statistics, and multi-scale aggregation
886 diagnostics indicates that the principal stagnation patterns identified for the Nile Delta are
887 generally robust within the methodological framework adopted in this study.

888 **8 Future Research Directions**

889 The results of this study highlight several priorities for future research aimed at improving
890 the physical understanding of atmospheric stagnation over low-relief coastal–continental
891 environments such as the Nile Delta. The analyses indicate that stagnation variability across
892 the region is strongly controlled by near-surface ventilation efficiency and boundary-layer
893 stability, as demonstrated by the strong inverse relationship between stagnation frequency
894 and surface wind speed. Future investigations should therefore focus on clarifying the



895 dynamical processes linking regional circulation variability with lower-tropospheric
896 ventilation over the Delta. In particular, the strong statistical linkage identified between
897 stagnation frequency and near-surface wind speed highlights the need for future studies to
898 better resolve the processes governing regional ventilation efficiency over the Nile Delta.

899 High-resolution regional climate modeling provides an important pathway for advancing this
900 understanding. Numerical simulations using mesoscale models such as the Weather Research
901 and Forecasting model (WRF) and its chemistry configuration (WRF-Chem) can resolve
902 atmospheric processes at kilometer-scale spatial resolution and sub-daily temporal scales.
903 These simulations can explicitly represent mesoscale circulation features that are often
904 smoothed in reanalysis datasets, including the inland penetration of Mediterranean sea-
905 breeze systems and thermally driven circulations over the Delta plains. Such modeling
906 experiments would allow detailed examination of the diurnal evolution of the planetary
907 boundary layer and help quantify how variations in boundary-layer depth, stability, and
908 turbulent mixing influence stagnation persistence during weak-wind conditions.

909 Further research should also investigate the sensitivity of stagnation regimes to variations in
910 regional pressure gradients between the Mediterranean Sea and the continental interior.
911 Changes in these gradients influence surface wind regimes and therefore the efficiency of
912 horizontal ventilation across the Delta. Particular attention should be given to how projected
913 modifications in regional wind fields may alter ventilation efficiency and stagnation
914 persistence. Understanding this relationship is essential for interpreting the strong statistical
915 association identified in this study between stagnation frequency and near-surface wind
916 speed.

917 Satellite remote sensing offers additional opportunities for examining the environmental
918 consequences of stagnation events. Observations from instruments such as Sentinel-5P and
919 MODIS provide valuable information on atmospheric composition, aerosol loading, and land
920 surface characteristics. When combined with ground-based meteorological and air-quality
921 observations, these datasets can improve understanding of how thermally stable conditions
922 influence pollutant accumulation and dispersion across the Nile Delta.

923 Future studies should also assess how projected changes in large-scale circulation may
924 influence stagnation regimes under continued climate warming. Climate projection
925 frameworks such as CMIP6 provide a suitable basis for evaluating potential modifications in



926 Mediterranean pressure gradients, regional wind regimes, and seasonal atmospheric stability
927 under emission scenarios such as SSP2-4.5 and SSP5-8.5.

928 Urban expansion across the Nile Delta represents another factor that warrants further
929 investigation. Changes in surface roughness, thermal properties, and land-surface energy
930 exchange influence boundary-layer development and local ventilation efficiency. High-
931 resolution urban climate simulations could therefore clarify how urban growth affects
932 turbulent mixing and air-mass renewal within major Delta cities.

933 Integrating stagnation diagnostics into air-quality early-warning systems and urban planning
934 frameworks may also provide practical benefits. Incorporating atmospheric ventilation
935 considerations into urban design could improve natural air exchange and reduce
936 environmental impacts associated with persistent stagnation conditions in rapidly expanding
937 Delta cities.

938 **9 Conclusion**

939 This study provides a quantitative climatological assessment of the spatial and temporal
940 characteristics of air stagnation across the Nile Delta during the period 1980–2020 using
941 high-resolution reanalysis datasets and spatial statistical analysis. The results demonstrate
942 that atmospheric stagnation over the region represents a persistent climatic feature rather than
943 an isolated meteorological occurrence. Clear spatial and seasonal patterns were identified,
944 with stagnation reaching its highest frequency during summer when weakened pressure
945 gradients and the eastward extension of the subtropical high reduce horizontal ventilation and
946 promote stable boundary-layer conditions.

947 The analysis further indicates a gradual increase in stagnation frequency over the study
948 period, particularly across the central and southern sectors of the Delta where urban
949 expansion is most pronounced. This tendency reflects the combined influence of declining
950 near-surface wind speeds, enhanced boundary-layer stability, and regional warming. The
951 strong inverse relationship identified between stagnation frequency and surface wind speed
952 highlights the dominant role of horizontal ventilation in regulating stagnation variability
953 across the region.

954 Spatial contrasts between coastal and inland areas further illustrate the influence of regional
955 circulation processes. Coastal locations benefit from persistent marine ventilation associated



956 with Mediterranean sea-breeze circulation, while inland sectors experience weaker
957 ventilation and more frequent stagnation conditions. These differences emphasize the
958 importance of mesoscale atmospheric processes in shaping the regional distribution of
959 stagnation events across the Delta.

960 From a methodological perspective, the study demonstrates the value of combining high-
961 resolution reanalysis datasets such as ERA5 and ERA5-Land with spatial analytical
962 techniques for diagnosing mesoscale atmospheric variability. This integrated framework
963 enables the identification of regional stagnation patterns and their relationship to boundary-
964 layer processes and surface wind regimes.

965 Overall, the findings indicate that the Nile Delta represents a region of increasing sensitivity
966 to atmospheric stagnation under ongoing climatic and environmental change. Understanding
967 the dynamics that control ventilation efficiency and boundary-layer stability over the Delta is
968 therefore essential for assessing future environmental conditions in this densely populated
969 coastal region.

970

971 **Declarations**

972 **Funding:** This research received no external funding.

973 **Ethics approval and consent to participate:** Not required for this study.

974 **Consent for publication:** Not applicable.

975 **Competing interests:** The author declares no competing interests.

976 **Author contributions:** H.B. conceived the study, conducted the analysis, and
977 wrote the manuscript. S.A. contributed to data processing, visualization, and
978 methodology. Both authors interpreted the results and approved the final version.

979 **Data and materials availability:** All data used in this study are included within
980 the article. Additional information is available from the corresponding author upon
981 reasonable request.

982

983

984

985



986 **References**

- 987 Abdelaal, M. M.: Rainfall characteristics in Egypt from 1960 to 2017: patterns,
988 variability, driving mechanisms, and impacts, in: *Hydroclimatic Extremes in the*
989 *Middle East and North Africa*, Elsevier, 149–175, [https://doi.org/10.1016/B978-](https://doi.org/10.1016/B978-0-12-824130-1.00001-1)
990 [0-12-824130-1.00001-1](https://doi.org/10.1016/B978-0-12-824130-1.00001-1), 2024.
- 991 Agarwal, P.: Quantifying drivers and impacts of an extreme particulate matter pollution
992 episode in India, Ph.D. thesis, University of Edinburgh,
993 <https://doi.org/10.7488/era/5364>, 2024.
- 994 Ahmed, S. O., Mazloun, R., and Abou-Ali, H.: Spatiotemporal interpolation of air
995 pollutants in the Greater Cairo and the Delta, Egypt, *Environ. Res.*, 160, 27–34,
996 <https://doi.org/10.1016/j.envres.2017.09.005>, 2018.
- 997 Azorin-Molina, C., Guijarro, J. A., McVicar, T. R., Trewin, B. C., Frost, A. J., and Chen,
998 D.: An approach to homogenize daily peak wind gusts: An application to the
999 Australian series, *Int. J. Climatol.*, 39, 2260–2277,
1000 <https://doi.org/10.1002/joc.5949>, 2019.
- 1001 Brune, S., Keller, J. D., and Wahl, S.: Evaluation of wind speed estimates in reanalyses
1002 for wind energy applications, *Adv. Sci. Res.*, 18, 33–39,
1003 <https://doi.org/10.5194/asr-18-115-2021>, 2021.
- 1004 Central Agency for Public Mobilization and Statistics (CAPMAS): *Egypt in Figures*
1005 *2023*, CAPMAS, Cairo, Egypt, 2023.
- 1006 Cerro, J. C., Cerda, V., and Pey, J.: Trends of air pollution in the Western Mediterranean
1007 Basin from a 13-year database: A research considering regional, suburban and
1008 urban environments, *Atmos. Environ.*, 122, 346–356,
1009 <https://doi.org/10.1016/j.atmosenv.2014.12.014>, 2015.
- 1010 El-Askary, H., Gautam, R., Singh, R. P., and Kafatos, M.: Dust storms detection over
1011 the Indo-Gangetic basin using multi sensor data, *Adv. Space Res.*, 37, 728–733,
1012 <https://doi.org/10.1016/j.asr.2005.03.134>, 2006.
- 1013 El-Metwally, M., Alfaro, S. C., Wahab, M. A., Zakey, A. S., and Chatenet, B.: Seasonal
1014 and inter-annual variability of the aerosol content in Cairo (Egypt) as deduced
1015 from the comparison of MODIS aerosol retrievals with direct AERONET
1016 measurements, *Atmos. Res.*, 97, 14–25,
1017 <https://doi.org/10.1016/j.atmosres.2010.03.003>, 2010.
- 1018 Fiore, A. M., Naik, V., and Leibensperger, E. M.: Air quality and climate connections, *J.*
1019 *Air Waste Manage. Assoc.*, 65, 645–685,
1020 <https://doi.org/10.1080/10962247.2015.1040526>, 2015.
- 1021 Frihy, O. E. and El-Sayed, W. R.: Vulnerability risk assessment and adaptation to
1022 climate change induced sea level rise along the Nile Delta coastal zone, Egypt,
1023 *Ocean Coast. Manage.*, 83, 14–22, <https://doi.org/10.1007/s11027-012-9418-y>,
1024 2013.



- 1025 Gelaro, R., McCarty, W., Suárez, M. J., Todling, R., Molod, A., Takacs, L., Randles, C.
1026 A., Darmenov, A., Bosilovich, M. G., Reichle, R., Wargan, K., Coy, L.,
1027 Cullather, R., Draper, C., Akella, S., Buchard, V., Conaty, A., da Silva, A. M.,
1028 Gu, W., Kim, G., Koster, R., Lucchesi, R., Merkova, D., Nielsen, J. E., Partyka,
1029 G., Pawson, S., Putman, W., Rienecker, M., Schubert, S. D., Sienkiewicz, M.,
1030 and Zhao, B.: The Modern-Era Retrospective Analysis for Research and
1031 Applications, Version 2 (MERRA-2), *J. Climate*, 30, 5419–5454,
1032 <https://doi.org/10.1175/JCLI-D-16-0758.1>, 2017.
- 1033 Hamed, K. H. and Rao, A. R.: A modified Mann–Kendall trend test for autocorrelated
1034 data, *J. Hydrol.*, 204, 182–196, 1998.
- 1035 Hassaan, M. A., Abdallah, S. M., Shalaby, E. S. A., and Ibrahim, A. A.: Assessing
1036 vulnerability of densely populated areas to air pollution using Sentinel-5P
1037 imageries: a case study of the Nile Delta, Egypt, *Sci. Rep.*, 13, 17406,
1038 <https://doi.org/10.1038/s41598-023-44186-4>, 2023.
- 1039 Hereher, M., Eissa, R., Alqasemi, A., and Elmahdy, S.: Assessment of air pollution at
1040 Greater Cairo in relation to the spatial variability of surface urban heat island,
1041 *Environ. Sci. Pollut. Res.*, 29, 69842–69859, [https://doi.org/10.1007/s11356-](https://doi.org/10.1007/s11356-021-17383-9)
1042 [021-17383-9](https://doi.org/10.1007/s11356-021-17383-9), 2022.
- 1043 Hersbach, H., Bell, B., Berrisford, P., Hirahara, S., Horányi, A., Muñoz-Sabater, J.,
1044 Nicolas, J., Peubey, C., Radu, R., Schepers, D., Simmons, A., Soci, C., Abdalla,
1045 S., Abellan, X., Balsamo, G., Bechtold, P., Biavati, G., Bidlot, J., Bonavita, M.,
1046 Chiara, G., Dahlgren, P., Dee, D., Diamantakis, M., Dragani, R., Flemming, J.,
1047 Forbes, R., Fuentes, M., Geer, A., Haimberger, L., Healy, S., Hogan, R., Hólm,
1048 E., Janisková, M., Keeley, S., Laloyaux, P., Lopez, P., Lupu, C., Radnoti, G., de
1049 Rosnay, P., Rozum, I., Vamborg, F., Villaume, S., and Thépaut, J.-N.: The ERA5
1050 global reanalysis, *Q. J. Roy. Meteor. Soc.*, 146, 1999–2049,
1051 <https://doi.org/10.1002/qj.3803>, 2020.
- 1052 Horton, D. E., Harshvardhan, and Diffenbaugh, N. S.: Response of air stagnation
1053 frequency to anthropogenically enhanced radiative forcing, *Proc. Natl. Acad.*
1054 *Sci. USA*, 109, 11175–11180, <https://doi.org/10.1073/pnas.1207587109>, 2012.
- 1055 Horton, D. E., Skinner, C. B., Singh, D., and Diffenbaugh, N. S.: Occurrence and
1056 persistence of future atmospheric stagnation events, *Nat. Clim. Change*, 4, 698–
1057 703, <https://doi.org/10.1038/nclimate2272>, 2014.
- 1058 Hu, Y., Tao, L., and Liu, J.: Poleward expansion of the Hadley circulation in CMIP5
1059 simulations, *Adv. Atmos. Sci.*, 30, 790–795, [https://doi.org/10.1007/s00376-012-](https://doi.org/10.1007/s00376-012-2187-4)
1060 [2187-4](https://doi.org/10.1007/s00376-012-2187-4), 2013.
- 1061 Huang, Q., Cai, X., Song, Y., and Zhu, T.: Air stagnation in China (1985–2014):
1062 climatological mean features and trends, *Atmos. Chem. Phys.*, 17, 7793–7805,
1063 <https://doi.org/10.5194/acp-17-7793-2017>, 2017.



- 1064 Huang, Q., Cai, X., Wang, J., Song, Y., and Zhu, T.: Climatological study of the
1065 boundary-layer air stagnation index for China and its relationship with air
1066 pollution, *Atmos. Chem. Phys.*, 18, 7573–7593, [https://doi.org/10.5194/acp-18-](https://doi.org/10.5194/acp-18-7573-2018)
1067 [7573-2018](https://doi.org/10.5194/acp-18-7573-2018), 2018.
- 1068 Intergovernmental Panel on Climate Change (IPCC): *Climate Change 2021: The*
1069 *Physical Science Basis*, Cambridge Univ. Press, Cambridge,
1070 <https://doi.org/10.1017/9781009157896>, 2021.
- 1071 Jacob, D. J. and Winner, D. A.: Effect of climate change on air quality, *Atmos. Environ.*,
1072 43, 51–63, <https://doi.org/10.1016/j.atmosenv.2008.09.051>, 2009.
- 1073 Jacob, D. J., Logan, J. A., and Murti, P. P.: Effect of rising Asian emissions on surface
1074 ozone in the United States, *Geophys. Res. Lett.*, 26, 2175–2178,
1075 <https://doi.org/10.1029/1999GL900450>, 1999.
- 1076 Leung, L. R. and Gustafson, W. I.: Potential regional climate change and implications to
1077 US air quality, *Geophys. Res. Lett.*, 32, L16711,
1078 <https://doi.org/10.1029/2005GL022911>, 2005.
- 1079 Li, Q., Zhang, H., Cai, X., and Song, Y.: The impacts of the atmospheric boundary layer
1080 on regional haze in North China, *npj Clim. Atmos. Sci.*, 4, 54,
1081 <https://doi.org/10.1038/s41612-021-00165-y>, 2021.
- 1082 Li, Z., Zhou, Y., Wan, B., Chen, Q., Huang, B., Cui, Y., and Chung, H.: The impact of
1083 urbanization on air stagnation: Shenzhen as case study, *Sci. Total Environ.*, 664,
1084 347–362, <https://doi.org/10.1016/j.scitotenv.2019.01.232>, 2019.
- 1085 Lu, J., Vecchi, G. A., and Reichler, T.: Expansion of the Hadley cell under global
1086 warming, *Geophys. Res. Lett.*, 34, L06805,
1087 <https://doi.org/10.1029/2006GL028443>, 2007.
- 1088 Majidi, F., Sabetghadam, S., Gharaylou, M., and Rezaian, R.: Evaluation of the
1089 performance of ERA5, ERA5-Land and MERRA-2 reanalysis to estimate snow
1090 depth over a mountainous semi-arid region in Iran, *J. Hydrol. Reg. Stud.*, 58,
1091 102246, <https://doi.org/10.1016/j.ejrh.2025.102246>, 2025.
- 1092 McVicar, T. R., Roderick, M. L., Donohue, R. J., Li, L. T., Van Niel, T. G., Thomas, A.,
1093 Grieser, J., Jhajharia, D., Himri, Y., Mahowald, N. M., Mescherskaya, A. V.,
1094 Kruger, A. C., Rehman, S., and Dinpashoh, Y.: Global review and synthesis of
1095 trends in observed terrestrial near-surface wind speeds: Implications for
1096 evaporation, *J. Hydrol.*, 416–417, 182–205,
1097 <https://doi.org/10.1016/j.jhydrol.2011.10.024>, 2012.
- 1098 Molina, L. T.: Introductory lecture: air quality in megacities, *Faraday Discuss.*, 226, 9–
1099 52, <https://doi.org/10.1039/D0FD00123F>, 2020.
- 1100 Nashwan, M. S., Shahid, S., and Abd Rahim, N.: Unidirectional trends in annual and
1101 seasonal climate and extremes in Egypt, *Theor. Appl. Climatol.*, 137, 1181–
1102 1198, <https://doi.org/10.1007/s00704-018-2498-1>, 2019.



- 1103 Ordoñez, C., Mathis, H., Furger, M., Henne, S., Hüglin, C., Staehelin, J., and Prévôt, A.
1104 S. H.: Changes of daily surface ozone maxima in Switzerland in all seasons
1105 from 1992 to 2002 and discussion of summer 2003, *Atmos. Chem. Phys.*, 5,
1106 1187–1203, <https://doi.org/10.5194/acp-5-1187-2005>, 2005.
- 1107 Ouassanouan, Y., Simonneaux, V., Kharrou, M. H., Fakir, Y., Baba, M. W., Hssaine, B.
1108 A., and Chehbouni, A.: Downscaled ERA5-Land addresses agrometeorological
1109 data scarcity in North African basins, *Sci. Rep.*, 15, 38533,
1110 <https://doi.org/10.1038/s41598-025-20552-2>, 2025.
- 1111 Raj, S., Paul, S. K., Chakraborty, A., and Kuttippurath, J.: Anthropogenic forcing
1112 exacerbating the urban heat islands in India, *J. Environ. Manage.*, 257, 110006,
1113 <https://doi.org/10.1016/j.jenvman.2019.110006>, 2020.
- 1114 Ramon, J., Lledó, L., Torralba, V., Soret, A., and Doblás-Reyes, F. J.: What global
1115 reanalysis best represents near-surface winds?, *Q. J. Roy. Meteor. Soc.*, 145,
1116 3236–3251, <https://doi.org/10.1002/qj.3616>, 2019.
- 1117 Ryu, Y. H. and Min, S. K.: Anthropogenic warming degrades spring air quality in
1118 Northeast Asia by enhancing atmospheric stability and transboundary transport,
1119 *npj Clim. Atmos. Sci.*, 7, 50, <https://doi.org/10.1038/s41612-024-00603-7>, 2024.
- 1120 Sarria, F. R., Palma, R. M., Amores, T. P., García-Melgar, P., Montero-Gutiérrez, M.,
1121 and Delgado, M. G.: Ventilation results and CFD model formulation for street
1122 canyons applied to climate control strategies, in: *Getting to Zero—Beyond
1123 Energy Transition Towards Carbon-Neutral Mediterranean Cities*, Springer,
1124 Cham, 241–252, https://doi.org/10.1007/978-3-031-82323-7_20, 2025.
- 1125 Seidel, D. J., Fu, Q., Randel, W. J., and Reichler, T. J.: Widening of the tropical belt in a
1126 changing climate, *Nat. Geosci.*, 1, 21–24, <https://doi.org/10.1038/ngeo.2007.38>,
1127 2008.
- 1128 Stanley, D. J. and Warne, A. G.: Nile Delta in its destruction phase, *J. Coast. Res.*, 14,
1129 795–825, 1998.
- 1130 Tai, A. P., Mickley, L. J., and Jacob, D. J.: Impact of 2000–2050 climate change on fine
1131 particulate matter (PM_{2.5}) air quality inferred from a multi-model analysis of
1132 meteorological modes, *Atmos. Chem. Phys.*, 12, 11329–11337,
1133 <https://doi.org/10.5194/acp-12-11329-2012>, 2012.
- 1134 Vautard, R., Cattiaux, J., Yiou, P., Thépaut, J.-N., and Ciais, P.: Northern Hemisphere
1135 atmospheric stilling partly attributed to an increase in surface roughness, *Nat.
1136 Geosci.*, 3, 756–761, <https://doi.org/10.1038/ngeo979>, 2010.
- 1137 Wang, J. X. and Angell, J. K.: *Air stagnation climatology for the United States (1948–
1138 1998)*, NOAA Air Resources Laboratory Atlas No. 1, NOAA, Silver Spring,
1139 MD, USA, 1999.
- 1140 Wang, L., Li, M., Wang, Q., Li, Y., Xin, J., Tang, X., and Wang, Y.: Air stagnation in
1141 China: Spatiotemporal variability and differing impact on PM_{2.5} and O₃ during



1142 2013–2018, *Sci. Total Environ.*, 819, 152778,
1143 <https://doi.org/10.1016/j.scitotenv.2021.152778>, 2022.
1144 Wang, Y., Guo, Z., and Han, J.: The relationship between urban heat island and air
1145 pollutants and them with influencing factors in the Yangtze River Delta, China,
1146 *Ecol. Indic.*, 129, 107976, <https://doi.org/10.1016/j.ecolind.2021.107976>, 2021.
1147 Zanaty, N., Ibrahim, N., Ramadan, H. K. A., Ahmad, A. A., and Saad-Hussein, A.:
1148 Significance of climate change in the emergence of human fascioliasis in Upper
1149 Egypt, *Trop. Dis. Travel Med. Vaccines*, 10, 24, [https://doi.org/10.1186/s40794-](https://doi.org/10.1186/s40794-024-00234-z)
1150 [024-00234-z](https://doi.org/10.1186/s40794-024-00234-z), 2024.
1151 Zhou, M., Xie, Y., Wang, C., Shen, L., and Mauzerall, D. L.: Impacts of current and
1152 climate-induced changes in atmospheric stagnation on Indian surface PM_{2.5}
1153 pollution, *Nat. Commun.*, 15, 7448, [https://doi.org/10.1038/s41467-024-51462-](https://doi.org/10.1038/s41467-024-51462-y)
1154 [y](https://doi.org/10.1038/s41467-024-51462-y), 2024.
1155 Zittis, G., Hadjinicolaou, P., Almazroui, M., Bucchignani, E., Driouech, F., El Rhaz, K.,
1156 and Lelieveld, J.: Business-as-usual will lead to super and ultra-extreme
1157 heatwaves in the Middle East and North Africa, *npj Clim. Atmos. Sci.*, 4, 20,
1158 <https://doi.org/10.1038/s41612-021-00178-7>, 2021.
1159
1160
1161
1162
1163
1164